How Good Are Symmetric Triangular Synthetic Storms to Represent Real Events for Coastal Hazard Modelling

Enrico Duo[1], Marc Sanuy[2], José A. Jiménez[2] and Paolo Ciavola[1]

[1]Department of Physics and Earth Science, University of Ferrara, Ferrara, Italy

[2]Laboratori d'Enginyeria Marítima (LIM), Universitat Politècnica de Catalunya – Barcelona Tech, Barcelona, Spain

Corresponding author: E. Duo (duonrc@unife.it).

Abstract Coastal risk assessments rely on proper quantification of storm-induced erosion and flooding, and often involve calculations via numerical models. When the real time-series data of a storm are not available as forcing conditions and only bulk information is accessible, synthetic simplified time-evolutions are assumed. The most common approach in coastal studies uses a symmetric triangular storm shape, characterised by the assumptions that the peak of the waves occurs in the middle of the storm, and that the forcing varies linearly. This study aims to investigate this additional source of uncertainty in hazard estimation, using the XBeach-1D model, to assess the differences in simulated erosion and flooding associated with real and synthetic storm definitions. Analysis is performed for real conditions ranging from moderate to extreme at the Northern Adriatic and North-Western Mediterranean coasts, using beach profiles ranging from dissipative to reflective. The storm definitions generate considerable differences in terms of wave power and timing at the peak of the storm. When synthetic storms were applied, coastal hazards were not adequately reproduced in most of the simulated cases. The energy of the storms, profile characteristics, local storm climates, and water levels did not consistently influence the differences between the synthetic- and reality-based outputs.

Keywords Coastal Storm, Mediterranean Sandy Beaches, XBeach, Flooding, Erosion, Numeric Model Uncertainty

1 Introduction

The reliability of the quantification of a hazard component is crucial for coastal risk studies. Coastal inundation and erosion hazards must be satisfactorily evaluated, especially when managing local assessments on sandy beaches. As an example, the magnitudes of a water discharge inundating the hinterland or of an eroded sediment volume are important for adequately evaluating the associated consequences for exposed elements. Moreover, local managers are interested in quantitative information to design risk reduction measures, such as dikes or nourishments, and to prepare management plans.

Nowadays, hazard assessments largely rely on numerical model simulations. Models are indeed capable of reproducing a large amount of processes affecting the interaction between the beach morphology and the storm event, to provide results from multiple hazards (Roelvink and Reniers, 2012). Nonetheless, these models rely on assumptions and simplifications that may produce unreliable results when compared with observed coastal hazards. As an example, the main factors affecting the simulation of flooding in urbanised coastal areas are linked to the mathematical formulations, the topographic data and the forcing boundary conditions (Gallien et al., 2018). Generally, the degree of robustness of a numerical model is related to the data availability and reliability. This is valid for the information on the morphology of the beach, the characteristics of the sediment, and the hydrodynamics. Therefore, the storm event needs to be suitably described and included in the numerical models as forcing data. Continuous (observed or hindcasted) storm time-series data of waves and water levels (WLs) are extremely important for capturing the evolution of the event, and thus its dynamic interaction with the beach.

When continuous forcing time-series data are unavailable, the event is generally described through observed or assessed bulk information, e.g. maximum significant wave height (Hs), peak wave period (Tp), maximum WL (mean sea level+surge+tide), duration (Dur), and main direction (Dir). The lack of continuous data leads to the introduction of simplifications and assumptions to proceed with the analysis of the storm hazard impacts. The most simplified approaches calculate impacts directly using statistical bulk information (see Ranasinghe and Callaghan, 2017). However, accounting for wave and WL variations during the storm is necessary for feeding process-based models (see e.g. Roelvink et al., 2009). In these cases, the evolution of the storm must be defined by means of a synthetic shape, hereafter called a synthetic storm (SS), with the assumption that it is representative of the real storm (RS). SSs are regularly used to define the shape of probabilistic storm events (i.e. representative of a given return period). A first attempt to standardise a procedure for SS applications can be found in Carley and Cox (2003), wherein they proposed a synthetically-designed storm with exponential-like growth and decay phases, and a symmetrical evolution around the peak. This was obtained by assessing Hs exceedances over various durations and associated with different return periods. Simpler approaches have been proposed to adapt synthetic storm shapes to the development of real storms. The triangular shape (Boccotti, 2000; Fedele and Arena, 2009; Corbella and Stretch, 2012a; Laface et al., 2016) is the most frequently applied due to its simplicity, while some studies investigated other shapes, such as the parabola or the trapezoid (Martin Soldevilla et al., 2015; Lin Ye et al., 2016), as well as exponential laws (Laface and Arena, 2016). The most recent approaches focused on robust statistical analysis of wave time-series to model the storm evolution (Solari and Losada, 2018; Lira-Loarca et al., 2020) or to generate joint time-series of wave parameters (Jäger et al., 2019). With some exceptions, most of above-mentioned methods rely on the availability of the storm time-series to properly mimic the storm development. Among all of them, the simplest approach that is widely applied in coastal studies is the symmetric triangular synthetic storm (STSS) (e.g. McCall et al., 2010; Corbella and Stretch, 2012b). It represents the evolution of an event from bulk characteristics at the peak and in the storm duration. STSSs are often used to cover all of the possible combinations of forcing (including those not previously recorded) when hazard and risk assessment approaches are applied, by simulating a large number of realistic storm conditions (e.g. Poelhekke et al., 2016; Plomaritis et al., 2018; Sanuy et al., 2018; Santos et al., 2019).

Thus, the use of any type of SS represents a useful approach for coastal hazard assessments, and the use of an SS is recommended for planning purposes by Nielsen and Adamantidis (2007). However, SSs show some inherent limitations, and represent an additional source of uncertainty in the analyses. Although there are some studies analysing the performance of SSs to represent the storm climate (e.g. Lin-Ye et al., 2016) but only a few analyse their effect in modelling coastal hazards. Sánchez-Arcilla et al. (2009) compared computed erosion impacts from RSs and SSs in the Spanish Mediterranean. The study used schematised, linearly-varying Hs and Tp mimicking the shape of the RS, and thus would have had little practical application if only the bulk parameters were known (e.g. as in the case of the STSS). Callaghan et al. (2009) assessed the reliability of an approach proposed by Carley and Cox (2003) for erosion assessments at Narrabeen Beach (Sydney, Australia), by comparing erosion impacts computed from adopting statistical events (i.e. representative of given return periods and simulated with synthetically-designed storms) and statistics of measured impacts. This study found a tendency to underestimate computed eroded volumes (EVs) with return periods between three and ten years. However, the results in Callaghan et al. (2009) demonstrate two different components of the uncertainty: the use of the SS, and the uncertainty of the methodology for assigning probabilities to the hazard (e.g. Sanuy et al., 2019). Therefore, the effect of the synthetic approach on the uncertainty was not isolated. More recently, the performance of triangular synthetic storms (including the STSS) has been evaluated for reproducing damage progression (Martín-Hidalgo et al., 2014) and overtopping (Martín Soldevilla et al., 2015) in marine structures. Triangular SSs showed a good performance but, depending on the characteristics of the storm, they tend to overestimate or underestimate damage. No study has ever assessed the role of commonly-used SSs in the propagation of uncertainties when modelling both coastal inundation and erosion hazards.

Within this context, the main aim of this work is to investigate the differences in storm-induced erosion and inundation assessments associated with the definition of storms (i.e. RS versus SS time-series) when using numerical modelling for specific storm conditions. The focus of this study is on the use of the most common and straightforward way of defining a SS, i.e. the STSS. To this end, the magnitude of coastal flooding and erosion is assessed using an extensive dataset of RS data and equivalent synthetic representations. The obtained variations are analysed, and are characterised from the differences observed in the storms. The analysis is performed for real conditions typical of the Northern Adriatic and North-Western Mediterranean coasts (Figure 1a). These cover beach profiles ranging from dissipative to reflective, and are subjected to storm conditions ranging from moderate to extreme. Storm-induced hazards were simulated with the XBeach-1D model (Roelvink et al., 2009).

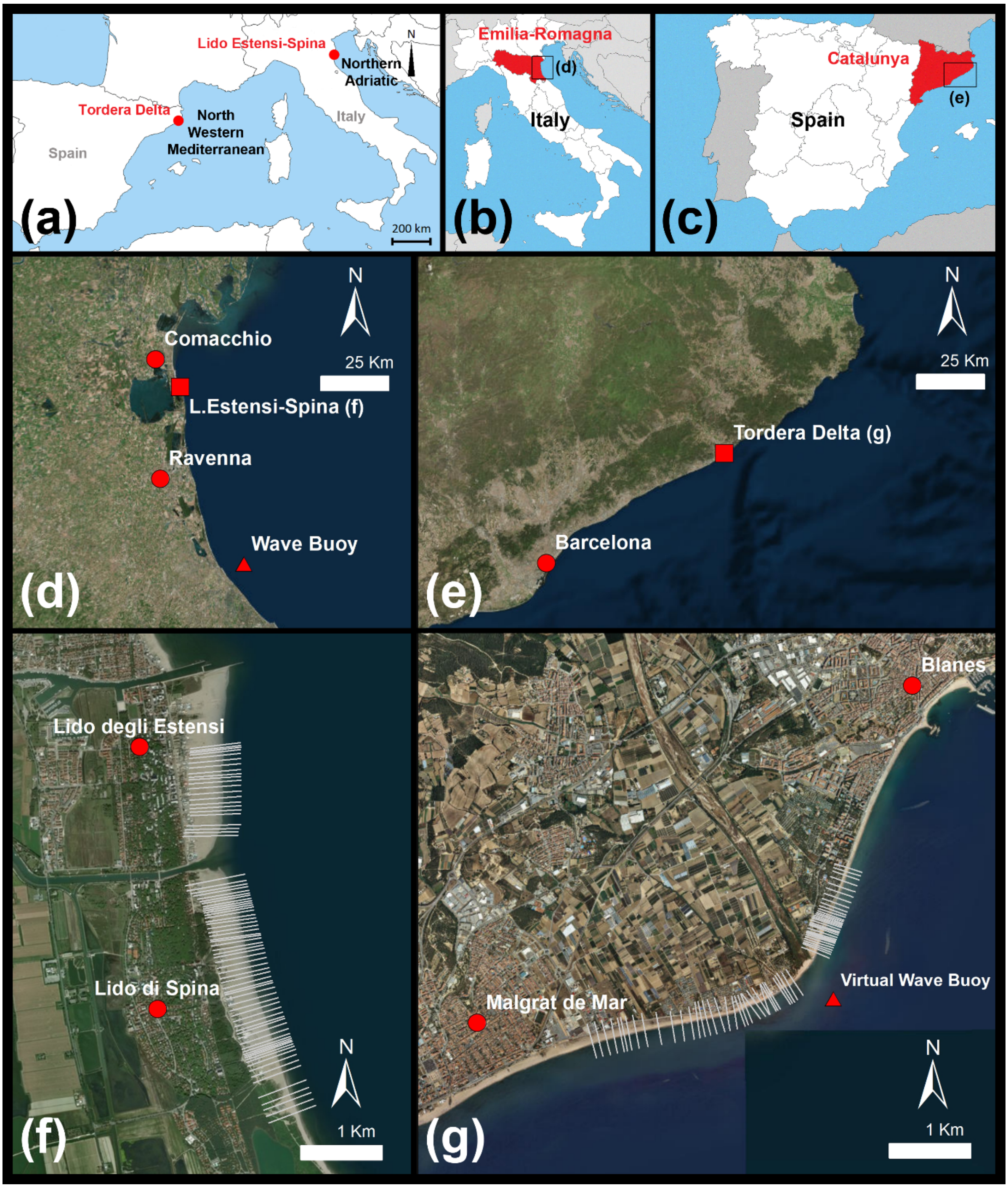

Figure 1. (a) Locations of the sites in the Northern Adriatic and North-Western Mediterranean Seas. The site (f), i.e. Lido Estensi-Spina is located on the (b,d) Emilia-Romagna (Italy) coast; whereas the site (g), i.e. the Tordera Delta is on the coast of (c,e) Catalunya (Spain). The main cities and towns are shown in (d), (e), (f), and (g) as circles. The locations of the wave buoys used to retrieve the wave data used in this study are shown in (d) and (e) as triangles. The partial tracks of the profiles used to select the representative data analysed in this study are shown in (f) and (g) as grey lines.

2 Methods and Data

2.1 Study area and data

The study area comprises two coastal stretches: in the Northern Adriatic (hereafter NA), Lido degli Estensi-Spina (Italy); and in the North-Western Mediterranean (hereafter NWM), the Tordera Delta (Spain) (Figure 1). These two areas are composed by fine and coarse sandy beaches, respectively. Both have been impacted by coastal storms, and they have already been classified as critical coastal sectors at the regional level (Armaroli and Duo, 2018; Jiménez et al. 2018). Sun-and-sand tourism is the main coastal economic sector at both sites and, owing to this, the related infrastructures and services (e.g. beach facilities, campsites, restaurants) are directly located on the beach, or in the immediate first part of the hinterland. Thus, these beaches provide space for accommodating beach users during the bathing season, and protection to the hinterland during the storm season. The general characteristics for each site, as well as the main references regarding site conditions, can be found in Table 1. The main data used in the analysis are shown in Table 2.

Table 1. General characteristics of study sites.

Site ID	Site	Sea Basin	Environment	Tidal range	Storm Surge	Waves	Main references for regional and local scales
Italy (IT)	Lido degli Estensi-Spina (Comacchio, Italy)	Northern Adriatic (NA)	Micro-tidal; Low-energetic; Dissipative.	neap: 0.3–0.4 m spring: 0.8–0.9 m	1-in-10 yrs: 0.72 m	Mean wave height: ~0.4 m; Max wave height: 4.6 m*.	Masina and Ciavola, 2011; Armaroli et al., 2012; Armaroli and Duo, 2018; Duo et al., 2018; Sanuy et al., 2018.
Spain (ES)	Tordera Delta (Blanes-Maresme, Spain)	North-Western Mediterranean (NWM)	Micro-tidal; Medium-energetic; Intermediate-reflective.	neap: 0.2–0.25 m spring: 0.3–0.4 m	1-in-10 yrs: 0.51 m	Mean wave height: ~0.7 m; Max wave height: 5.4 m**	Mendoza et al., 2011; Jiménez et al., 2018; Sanuy et al., 2018; Sanuy et al., 2019.

*recorded in February 2015 at the buoy in Figure 1f; **at the virtual node in Figure 1g.

Table 2. Summary information on the topo-bathymetric and wave datasets.

Site ID	Dataset	Type	Resolution	Period	Source
IT	Wave time-series (Hs, peak wave period (Tp), main direction (Dir))	Offshore buoy Wave buoy at 10 m depth (see Figure 1f)	0.5 h	2007–2018 (83% coverage)	ARPA E-R Available at: https://simc.arpae.it/dext3r/
	Topography digital surface model (DSM)	Lidar	1 × 1 m	October 2014	National Oil Company, Eni
	Nearshore Bathymetry	Lidar	1 × 1 m	2012	National Oil Company, Eni
	Offshore Bathymetry	Multibeam	1 × 1 m	2013	National Oil Company, Eni
ES	Wave time-serie (Hs, Tp, Dir)	DOW hindcast 20 m depth virtual buoy (see Figure 1g)	1 h	1960–2014	IH-Cantabria (Reguero et al., 2012; Camus et al., 2013)
	Bathymetry	Multibeam	1 × 1 m	2010	Spanish Ministry of Agriculture, Food and Environment
	Topography (DSM)	Lidar	1 × 1 m	2010	Institut Cartogràfic de Catalunya Available at: www.icgc.cat

2.2 Real storms

The first step in the analysis consists of defining the storms. To this end, storms were identified at each site by applying the peak-over-threshold (POT) method, with a double threshold for Hs, i.e. the 0.98 and 0.995 quantiles of the respective time-series, and by imposing a minimum

Dur based on local experience (see Table 3). The first Hs threshold (0.98 quantile) was used to calculate Dur, and to define the period between consecutive events. Events with shorter durations than the minimum Dur were not considered. Consecutive peaks with conditions under the threshold lasting less than the meteorological independence criterion (Table 1) were considered as part of the same storm event. The second Hs threshold was applied to identify the most significant storms, which are defined here as extreme events. Table 3 summarises main characteristics of the POT analysis for both sites. A total of 227 storms were identified to build the storm dataset (48 and 179 for the NA and NWM basins, respectively). As both wave datasets correspond to different water depths (10 m at NA, deep waters at NWM; see Table 2), the NA storms were linearly back-propagated to the deep waters to generate a consistent dataset.

Once the storms were identified, each storm was characterised through a set of wave parameters: Hs at the storm peak (Hs,max); Tp; Dir, and Dur. Then, the energy content (E) of the storm was calculated in the form of a proxy, as previously done by Mendoza et al. (2011), as:

$$E = \int Hs^2 dt \qquad (1)$$

where t is time in hours. Additionally, the wave power of the storm (P) was calculated to characterize its strength, since induced hazards depend on the rate at which wave energy is delivered (e.g. Burgint et al., 2017), and due to this it is becoming a main parameter to analyse temporal and spatial patterns in storminess (see e.g. Bromisrki and Cayan, 2015). P was calculated as:

$$P = \frac{\rho g}{8} \int Hs^2 \cdot Cg \; dt, \qquad (2)$$

Where t is time in seconds, ρ is the water density, g is the gravity, and Cg is the group velocity, which depends on Tp and water depth. Since storm definition is specified at the XBeach model outer boundary, and this is located at 20 m water depth, P was calculated by using the intermediate water version. Note that, in this study, E and P are calculated by integration over time for the entire duration of the storm, thus they units are [$m^2 \cdot s$] and [(W/m)·s], respectively.

Table 3 Characteristics of the peak-over-threshold (POT) analysis for identifying storms at each study site.

Site ID	Sea Basin	Hs 98% quantile	Hs 99.5% quantile	Minimum storm duration	Meteorological independence criterion	Nr. of storms
IT	NA	1.85 m	2.6 m	4 h	12 h	48
ES	NWM	2 m	2.6 m	6 h	72 h	179

2.3 Synthetic storms

To define a SS representing a real event, a simple shape describing the evolution of wave parameters during the storm must be selected (McCall, 2010; Poelhekke et al., 2016; Sanuy et al., 2018). As previously mentioned, this work focuses on the use of STSSs, where Hs linearly grows from the threshold value up to a Hs,max halfway through the storm duration. From there, it linearly decreases down to the threshold value (Figure 2).

To fully define the storm, it is necessary to assign a Tp to each Hs condition. This is a common problem in extreme wave analysis, when is necessary to associate a Tp with a height of a given return period (Mathiesen et al 1994). This is a site-specific problem which is solved by deriving empirical relationships, with copula-based approaches being widely used when real storm data are available (e.g. Corbella and Stretch, 2013). However, unless copula-based transformations for any site become available, the most usual way to do it is by using Tp-Hs deterministic relationships which are supplied together with extreme distributions of Hs (see e.g. Sanuy et al. 2019). For instance, in Spain, the State Ports Authority (Puertos del Estado) following Mathiesen et al (1994) provides a specific Tp-Hs relationship to be used together with the extreme wave height distribution for different areas along the Spanish coast. It is out of the scope of this work to analyse which is the best way to derive such relationships, thus, site specific relationships were applied. To assign the corresponding wave periods to each STSS, an empirically-derived Tp-Hs linear relationship, separately assessed for each storm dataset (Table 2) by using Hs and Tp bulk data at the peak of the events (for NA: $Tp[s]=1.32 \cdot Hs[m]+3.86$; for the NWM: $Tp[s]=1.75 \cdot Hs[m]+3.69$), is used (see e.g. Mathiesen et al., 1994). The linear fitting resulted in RMSEs ~0.9 s for both datasets, only considering the storm peaks. When evaluated for the entire timeseries (i.e., using the real Hs to model Tp), the RMSEs increased to ~1.15 s. With this, the synthetic wave period time-series will depend on the obtained empirical relation Tp-Hs, and on the adopted symmetric triangular shape of the synthetic Hs. Dir would correspond to the mean wave direction during the peak of the event, although in this study it is not considered. This is because in this analysis, the worst-case scenario is investigated, which corresponds to normal incidence. Since this study focuses on the schematization of the wave component, the effects of time-varying WLs (i.e. mean sea level+surges+tides) are ignored, and the WL is assumed to be constant for the duration of the storms.

To compare the SSs and RSs, a set of parameters have been selected. These parameters essentially characterise differences in storm shape (storm peak), E, Tp and P (see Table 4). The peak delay (PD) is defined as the time lag between the peaks of the RSs and SSs (Figure 2).

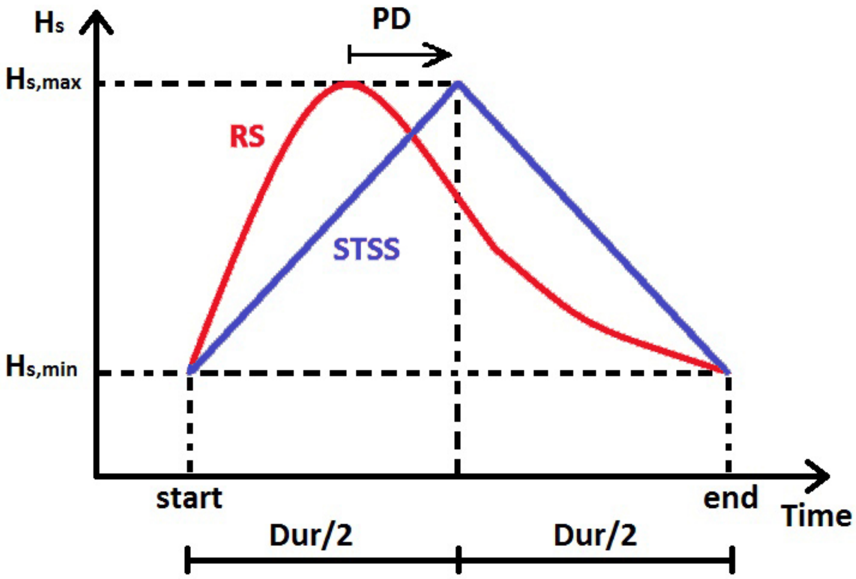

Figure 2. Real storm (RS) and symmetric triangular synthetic storm (STSS).

Table 4. Indicators to compare real and synthetic storms. Subscripts refer to real (r) and synthetic (s) storms.

Symbol	Name	Formula
ΔE	Storm energy relative difference	$100 \cdot (E_s - E_r)/E_r$
ΔTp	Peak period relative difference	$100 \cdot (Tp_s - Tp_r)/Tp_r$
ΔPD	Relative peak delay	$100 \cdot [t(Hs{,}max_s) - t(Hs{,}max_r)]/(0.5 \cdot Dur)$

ΔP	Storm wave power relative difference	$100 \cdot (P_s - P_r)/P_r$

2.4 Modelling of storm-induced hazards

To simulate storm-induced hazards, the process-based morphodynamic model XBeach (Roelvink et al., 2009) was used. It can be considered as a state-of-the-art model for simulating the impact of extreme events, and it is one of the most-used models for this purpose (e.g. McCall et al., 2010; Vousdoukas et al., 2012; Williams et al., 2015; Harley et al., 2016; Passeri et al., 2018). The model was applied in profile mode (1D), similarly to Vousdoukas et al. (2012) and Harley et al. (2016). Beach morphology, WL, waves, and water discharge were simulated and stored during the entire simulation of the storms. The parameters of the model were defined as the default values, except for morfac (5), D50, D90 (see Table 5), and bedfriction (white-colebrook-grainsize). In this way, the friction was calculated as a direct function of the sediment grain size.

In this application, topographic and bathymetric datasets (Table 2) of each site were merged to build a coastal digital terrain model, from which a significant number of profiles (i.e. 80 at the site in Italy (IT), Figure 1f; 67 at the site in Spain (ES), Figure 1g) were extracted to describe the local morphology of the beach in detail. At each site, the extracted profiles were classified into five groups, covering a range of local beach morphology. Grouping was performed by minimising the variability of all profiles with respect to an average profile, which was used to represent the beach morphology of the sector. This resulted in five average profiles for each site (Figure 3). All the profiles were artificially extended to a 20 m depth for consistency with the forcing time-series. The basic characteristics of the representative profiles and sediments (D50 and D90) are summarised in Table 5.

The storm conditions for the simulation consisted of 227 real events (see Section 2.2), and their 227 synthetic representations (see Section 2.3). Each real and synthetic event was simulated for each of the 10 profiles. To include the potential variability owing to the mean sea level conditions, three WL scenarios were defined (baseline WL, +0.25 m, +0.75 m). As a result, a total of 13620 simulations were computed.

The obtained results were the morphology and water discharge for each simulation. The water discharge (Q) time-series was extracted for each profile at the locations shown in Figure 3. The discharge positions were defined in areas that were not significantly affected by erosion for the entire dataset of simulations, and that were close enough to the shoreline to capture significant floodwater volumes.

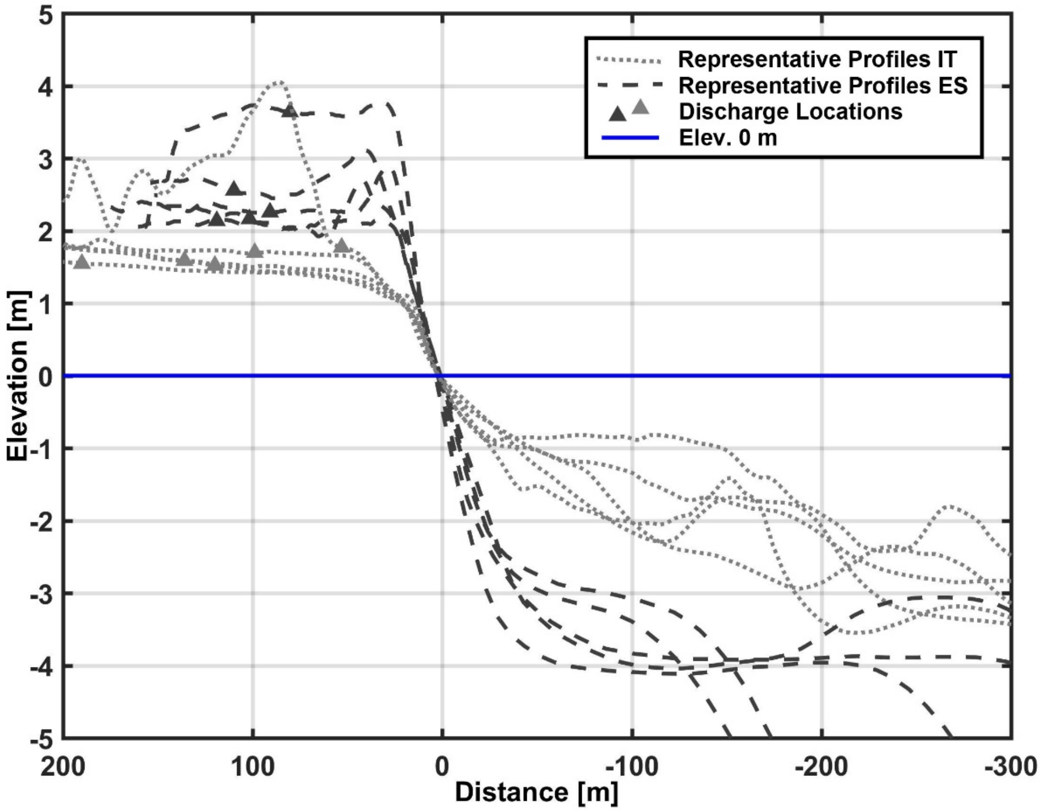

Figure 3. Overview of the profile dataset with indication of the discharge locations.

Table 5. Summary information on the profile dataset.

Site ID	Grain size [mm]		Representative average profile	Berm elevation	Slope	Dune	Bar
	D50	D90					
IT	0.23	0.3	1	1.06 m	0.043	Yes	Yes
			2	0.79 m	0.033	No	Yes
			3	1.00 m	0.031	No	Yes
			4	0.95 m	0.029	No	No
			5	1.11 m	0.005	No	Yes
ES	1.3	1.9	1	3.76 m	0.096	No	No
			2	2.89 m	0.099	No	No
			3	3.11 m	0.117	No	No
			4	2.70 m	0.117	No	No
			5	2.10 m	0.080	No	Yes

2.5 Analysis of simulated hazards

The EV of the emerged beach (i.e. from the shoreline to where erosion ends) was calculated by comparing the initial and post-storm profiles. The maximum and significant (i.e. the average of the highest third, to capture the average magnitude near the peak of the event) water discharges were calculated (as Qmax and Qs, respectively), as well as the total water volume (TWV) inundating the hinterland. These variables give quantitative information on both the peak of the storm (i.e. Qmax) and its event-integrated values (i.e. EV, Qs, and TWV).

For each variable, the differences between the real- and synthetic-driven outputs were assessed in an event-to-event manner through the expressions shown in Table 6. Positive values of the comparative variables indicate an over-estimation of the STSS in comparison to the RS, and vice versa. The use of relative differences can, however, generate misleading interpretations of the results for high-intensity events, as important absolute differences are smoothed relative to a large hazard output.

Table 6. Summary of the functions adopted to quantify the comparison between real- and synthetic-driven outputs.

Symbol	Name	Formula
ΔQD	Relative Peak Discharge Delay	$100 \cdot [t(Qmax_s) - t(Qmax_r)]/Dur$
ΔQ_s	Significant Discharge Relative Difference	$100 \cdot (Qs_s - Qs_r)/Qs_r$
ΔQ_{max}	Maximum Discharge Relative Difference	$100 \cdot (Qmax_s - Qmax_r)/Qmax_r$
ΔTWV	Total Water Volume Relative Difference	$100 \cdot (TWV_s - TWV_r)/TWV_r$
ΔEV	Eroded Volume Relative Difference	$100 \cdot (EV_s - EV_r)/EV_r$

3 Results

3.1 Storm characteristics

The application of the POT method to both datasets resulted in a total of 227 storms, 48 in the NA, and 179 in the NWM basin. As mentioned before, because the NA wave data were recorded at 10 m depth, the storm Hs values were back-propagated to the deep waters to obtain the corresponding offshore values and thereby generate a consistent dataset. The main characteristics of the identified storms (RS) at each site can be seen in Figure 4.

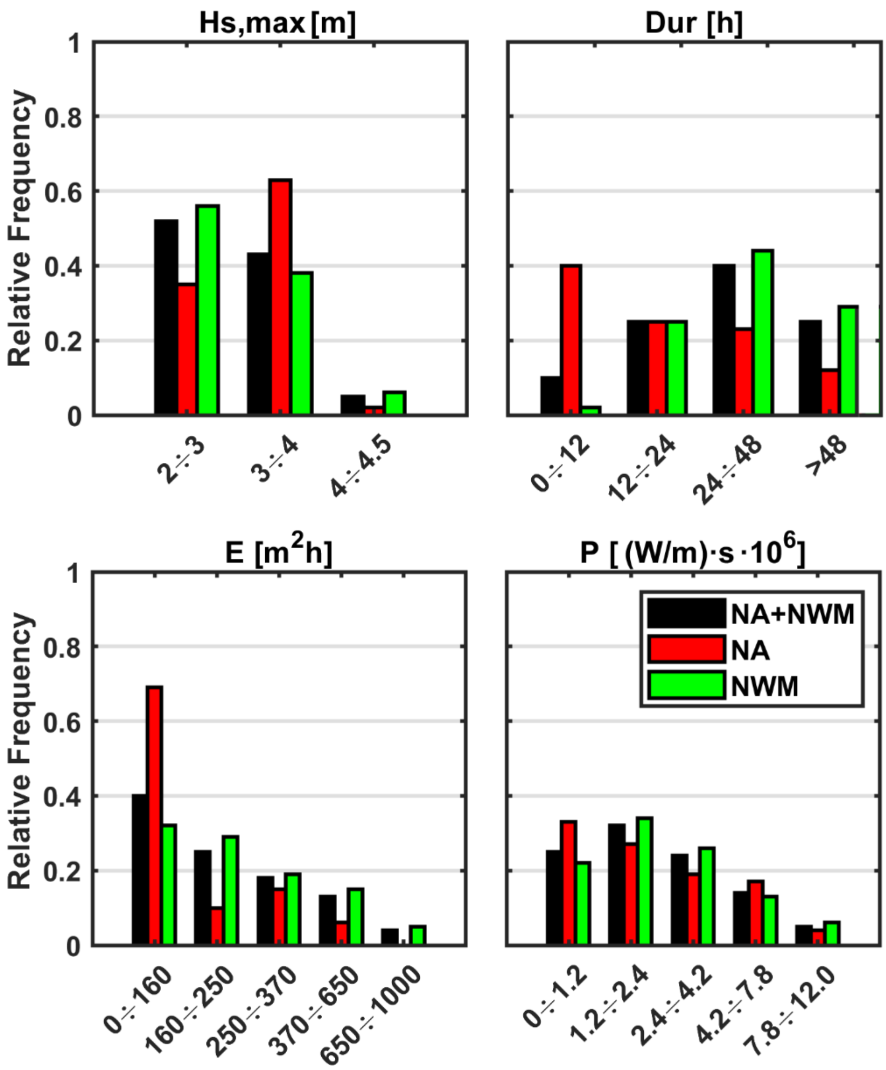

Figure 4. Main characteristics (wave height (Hs), duration (Dur), energy content (E), and wave power (P)) of RSs at both study sites. Black bars: relative frequency distribution for the whole dataset (NA+NWM); Red bars: relative conditional frequency distribution for Northern Adriatic (NA) storms; Green bars: relative conditional frequency distribution for North-Western Mediterranean (NWM) storms.

The comparison between a normalised shape of a RS versus its reproduction by means of the use of SSTS is shown in Figure 5. In addition, the median and associated 75% probability range (given by the 0.175 and 0.825 quantiles) of the normalised Hs time series of both storms are represented. As can be seen, the STSS mimics the typical Hs evolution, although some differences also occur. The average RS shows higher growth rates during a shorter Dur as compared to the average STSS. The average shape of the RS presents a plateau, indicating a natural variability in the occurrence of the peak during the storm. As a difference (and by definition), the average STSS shows a point peak at the middle of the storm. The shadowed areas in Figure 5 represent the variability of the Hs evolution during the storm, which, as expected, is larger for the RS.

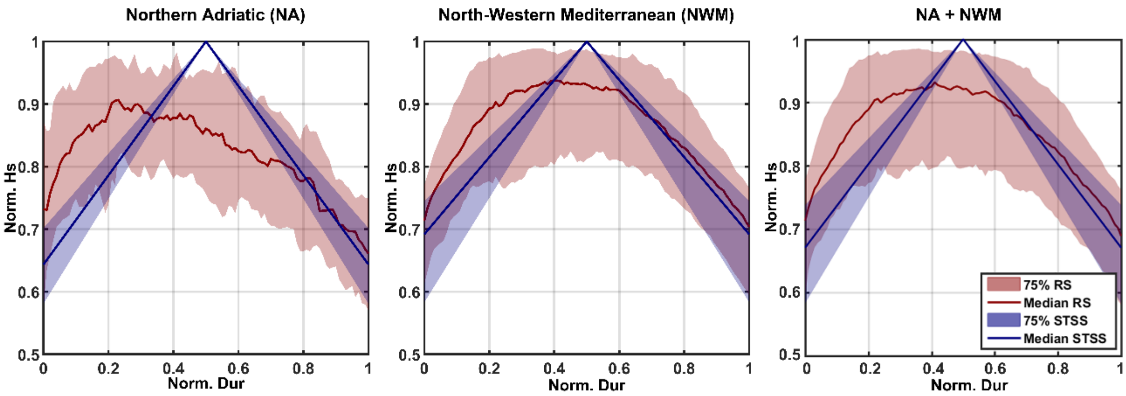

Figure 5. Significant Hs evolution for representative RSs and STSSs. From left to right: Northern Adriatic (NA) storms; North-Western Mediterranean (NWM) storms; and the whole dataset of storms (NA + NWM). Variables (Hs and Dur) are normalised. Solid lines correspond to the median for each storm type for the entire dataset, and the shadow area delineates the 0.175 and 0.825 quantiles.

Figure 6 illustrates a comparison between parameters defining RSs and SSs, in terms of the relative differences in PD, E, Tp, and P. As can be seen, the timing of the storm PD is reasonably well-captured, with more than 60 % of the total cases having a phase lag shorter than 6 h. In general terms, the adopted symmetric shape of the SSTS resulted in peaks slightly more frequently delayed with respect to the RS. However, when this parameter is measured in relative terms (ΔPD), the results indicate that 66% of storms present a phase lag of the peak that is longer than 20% of the Dur (as a reference, this corresponds to a phase lag of ~10 h on a 2-day storm). With respect to the E, approximately 40% of the cases were well-reproduced by using the STSS as they presented a relative difference smaller than 5%. The remaining cases presented both higher and lower energy values, with a slight tendency to underestimate E. Figure 6 also shows the differences in Tp between the STSS and RS. The relative difference for Tp is shown for the storm peaks only (Peak ΔTp), and as average over the whole duration of the storms (Mean ΔTp). By definition of the adopted approach, Peak ΔTp represents the difference due to the adoption of the Tp-Hs empirical relations (see Section 2.3) alone. In general, the results show that the adopted approach (i.e. empirical linear relation Tp-Hs) reasonably reproduces real wave periods at the storm peak (more than 50% of the cases presented an absolute relative difference lower than 5% in Peak Tp). The remaining cases show a slight tendency towards overestimating Tp at the storm peak. On the other hand, Mean ΔTp, which is calculated considering the whole duration of the storm, represents the combined difference due to the empirical relations and the synthetic storm shape. Results show a tendency of the approach to underestimate the Tp evolution of the storm, although the absolute values of Mean ΔTp are always lower than 20%, and for large part of the dataset (44%) are lower than 5%. The wave power presents relative differences (ΔP) lower than 5 % in less than 40 % of the cases. Actually, differences are contained within ± 20 % in almost 70 % of cases, with a tendency towards underestimation.

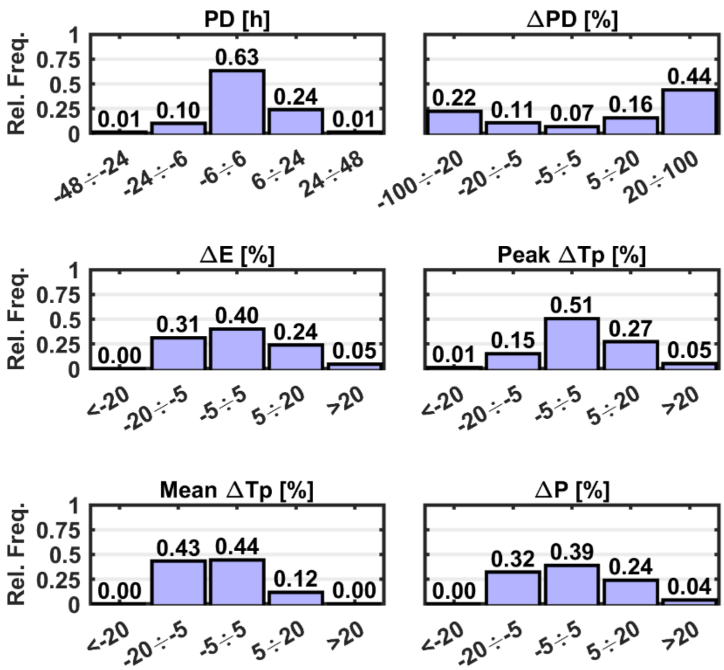

Figure 6 Variability in storm properties between STSS and RS according to the selected control parameters (Figure 2 and Table 4).

3.2 Storm-induced hazards

The previously-obtained differences in storm definition propagate to differences in hazard estimation. Figure 7 shows examples of model outputs from integrating the results of all of the performed simulations. The median of the position of the post-storm profile and normalised discharge time-series and the associated 75% probability ranges given by the 0.825 and 0.175 quantiles for the RS and STSS, respectively, are presented for two profiles of the dataset (one intermediate-reflective and one dissipative). The discharge normalization was implemented considering the average value between the real and synthetic Qmax for each combination storm-profile. The normalised discharges in Figure 7 provide information on how the STSS and RS compare in different phases of the storm relative to Dur, and cannot be interpreted to compare discharge peaks. This is because all STSSs have their peak in the centre of the storm, whereas only 7% of RSs do.

When assessing results across all profiles, the analysed events induced erosion and inundation hazards covering a large range of values (Figure 8). Thus, approximately 60% of the cases induced an inner EV larger than 60 m^3/m (this is equivalent to an average beachface retreat of approximately 30 m, assuming 2 m of beachface height), and more than 10% generated an erosion larger than 120 m^3/m (this is equivalent to an average beachface retreat of approximately 60 m, assuming 2 m of beachface height). With respect to inundation, more than approximately 25% of the events resulted in a TWV overtopping the beach and larger than 100 m^3/m (as reference, this is an average discharge of ~0.001 m^3/s over 24 h of storm).

The use of the STSS to represent the RS resulted in a general underestimation of storm-induced EVs (Figure 8), with approximately 20% of the cases underestimating the EV by more than 20%. With respect to the inundation hazard, the analysed variables were not properly simulated by using the STSS. As seen in Figure 7, the differences in the flood-related hazards are larger. In general, and independently of the beach type, the use of the STSS results in an under-prediction of the water discharge during most of the event, except during the central phase of the storm, when the discharge tends to be overestimated. This agrees with the phase lags obtained for the peak discharge (ΔQD, Figure 8). Overall, only a few cases resulted in a good reproduction of the maximum and/or significant discharges (Qmax and Qs), or the TWV. Notably, most cases underestimated or overestimated these variables with relative errors larger than 20%, with a higher tendency towards underestimation (Figure 8).

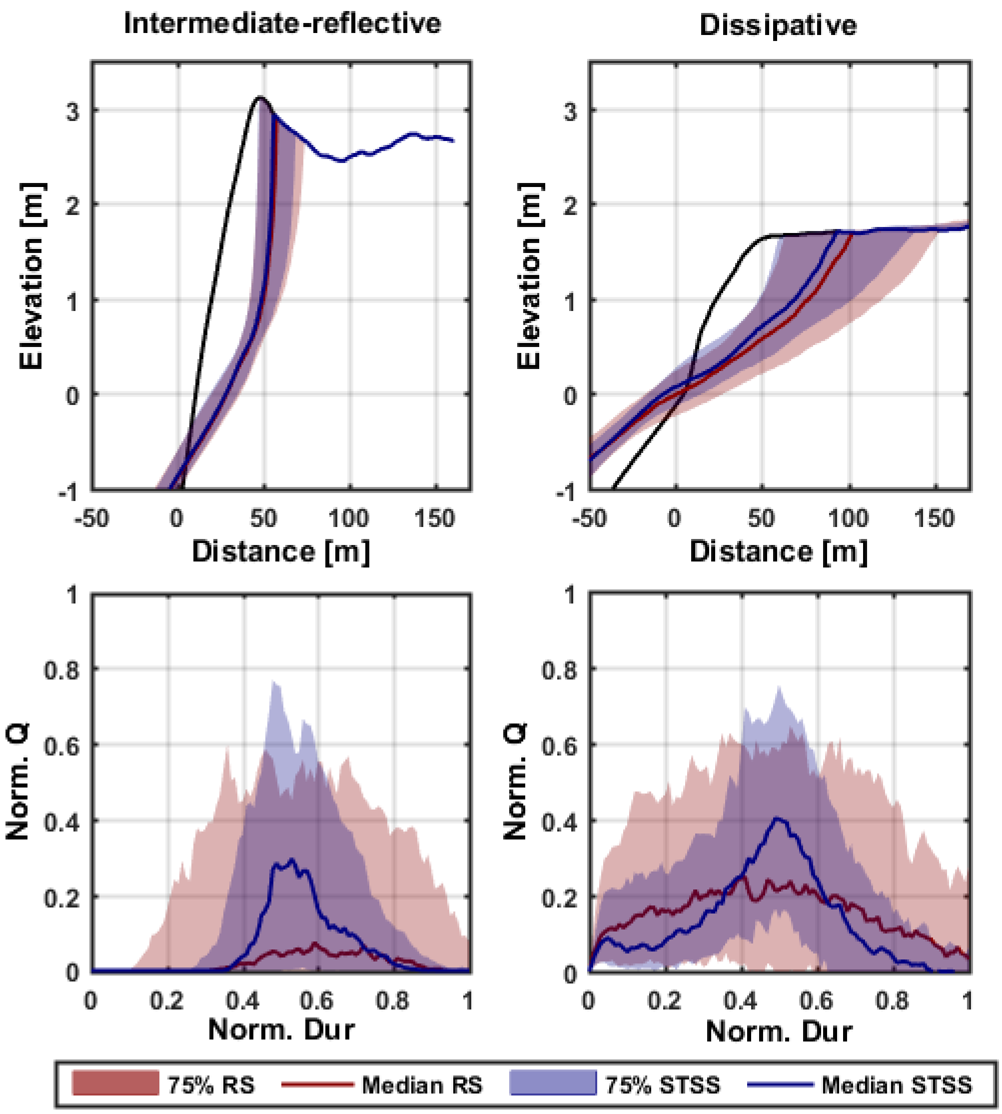

Figure 7. Real- (red) and synthetic-driven (blue) post-storm profiles calculated for the whole dataset of simulations for a predominantly intermediate-reflective (top-left) and dissipative (top-right) beach profile. Real- (red) and synthetic-driven (blue) normalised discharge time-series calculated for the whole dataset of simulations for a predominantly intermediate-reflective (bottom-left) and dissipative (bottom-right) beach profile. All graphs are represented by the median (solid line) and the 75% of the dataset (shaded area) given by the 0.175 and 0.825 quantiles.

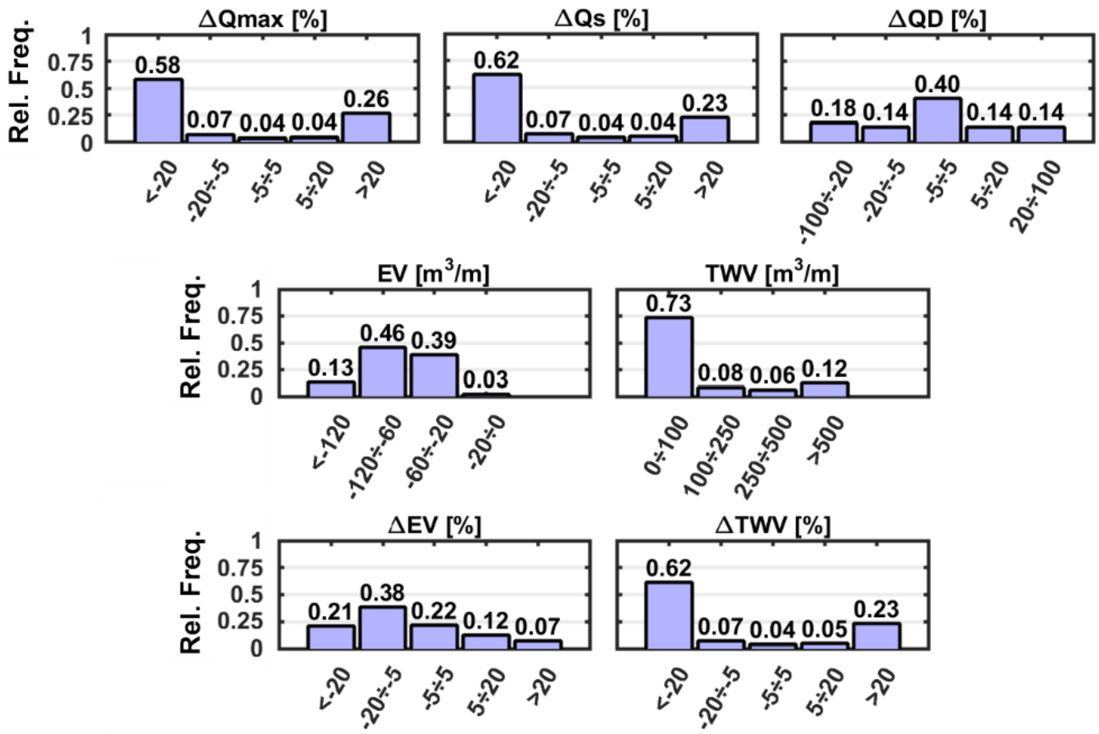

Figure 8. Variability in storm-induced hazards between STSS and RS according to the selected control parameters (Table 6).

4 Discussion

The analysis has shown that, although using synthetic time-series to represent wave forcing for simulating storm-induced coastal hazards is a widely-used approach (e.g. McCall et al., 2010; Corbella and Stretch, 2012b; Poelhekke et al., 2016; Plomaritis et al., 2018; Sanuy et al., 2018), the obtained results can significantly differ than those obtained using the real time-series they are intended to represent. This study represents the first attempt to quantify the uncertainty related to the use of these types of synthetic events in deterministic modelling.

The use of an STSS can be discussed in two different and complementary ways. The first one regards how well this approach represents the characteristics of an RS. The obtained results showed that, for this purpose, the use of an STSS provides a reasonable representation of reality, as it implies a perfect representation of Hs at Hs,max and the Dur of RSs. When the adopted shape has a potential influence on the magnitude of a variable to be characterised, the results begin to differ (e.g. E content). Thus, the selected triangular shape determines the PD between both approaches. As has been shown here, even when the analysed storms are retrieved from localised areas (two in this case) where the meteorology presents well-defined and stable patterns, the peak occurs at different phases of the RS development, depending on specific conditions. This results in a relatively wide fraction of the storm duration where the peaks can be verified, as contrasted with a single fixed point in the STSS. This prevents the proper representation of the storm growth and relaxation phases and, in consequence, potentially affects any process depending on these characteristics. Regarding wave periods, the adopted linear fitting approach (i.e., Tp-Hs) introduces additional errors. The RMSEs evaluated for the linear fit are low (~ 0.9 – 1.15 s; see Section 2.3) for both wave datasets and, as a consequence, the Tp at the storm peaks is reasonably well-captured (Peak ΔTp) because they are only affected by the uncertainty of the adopted linear model. However, because Tp values within the synthetic storm depend on the adopted storm shape – triangular in this case (see Section 2.3) – the reproduction of Tp during the entire storm was less accurate (Mean ΔTp). Since P depends on Hs (thus, on E) and Tp, errors in both variables are transferred to errors in P.

The second consideration regards how changes in storm properties are transferred to storm-induced hazards. As opposed to the previous parameters, according to the obtained results, the adopted STSS has important effects on the reproduction of the induced hazards. Indeed, the storm-induced erosion was properly captured in just 22% of cases, whereas the TWV inundating the hinterland was properly captured in only 4% of cases. The better representation of the erosion hazard is a consequence of the morphodynamic feedback taking place during the impact of the storm, where the modifications of the beach morphology affect beach overtopping. In consequence, errors in beach morphology reproduction will propagate (and expand) to beach inundation.

In this study, the differences in the EV (ΔEV) were strongly related with differences in P (ΔP) between the real and triangular time-series (Figure 9). Secondarily, ΔEV are related to differences in wave period (ΔTp), in storm energy (ΔE), and the delay of the peak (ΔPD). As expected, consistent under- and over-estimation of the wave power lead to under- and over-estimation of the eroded volume.. Thus, if the wave power is not well represented, models based on the average equations of mass and momentum cannot properly compute erosion and flooding. In this sense, it has to be considered that most of current definition of synthetic storms, and STSS in particular, are based on representing wave height and, in consequence, they do not necessarily conserve wave power during the storm. Notably, approaches to design SS based on P conservation may solve this issue, but they are not applicable when the only available information are the bulk characteristics (at the peak) of the storm event. In Figure 9, ΔE and Peak ΔTp are only moderately linked to ΔEV when considered separately, while the dependency is emphasized when considering Mean ΔTp. This suggests that both the initial assumptions, on the adopted synthetic shape and on the Tp-Hs relation, affect the proper assessment of EV. However the contribution of the adopted shape has a double impact as directly affecting E (i.e. through Hs) and the Tp time-series of the storm. Note that, the under-/over-estimation of the EV was also linked to the delay of the peak (ΔPD>20%) and storm peak anticipation (ΔPD<-20%) respectively.

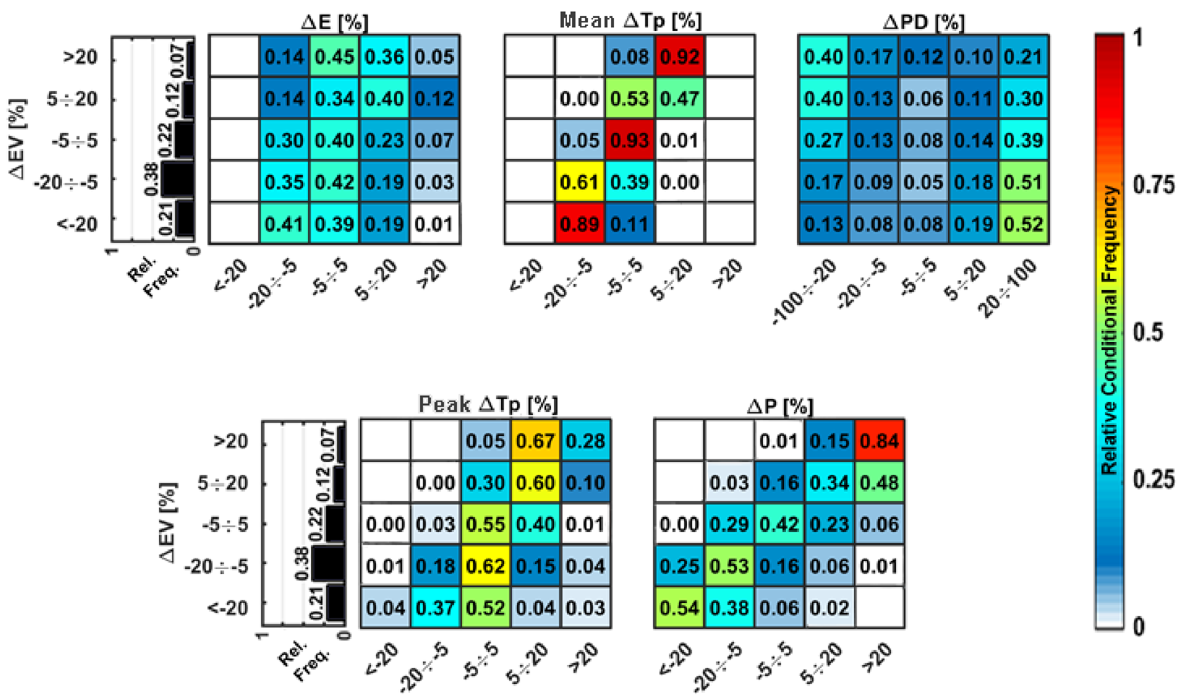

Figure 9. Relation between the eroded volume relative difference (ΔEV) with the variables describing the relative differences between the real and triangular time-series. The relative conditional frequency distributions are shown through coloured tables, where each row represents a conditioning range of ΔEV. On the left, top and bottom: distribution of eroded volume relative difference (ΔEV) for the whole dataset. From left to right, top to bottom: conditional distributions of energy relative difference (ΔE); period mean relative difference (Mean ΔTp); relative peak delay (ΔPD); period at the peak of the storm relative difference (ΔTp); and wave power relative difference (ΔP).

Sánchez-Arcilla et al. (2009) also compared the use of RSs and SSs to assess beach erosion using the Sbeach model (Larson and Kraus, 1989). In their study, they used simplified Hs and Tp time-series in linear segments following the evolution of the RSs, and thereby captured storm peaks. Their study showed an over-estimation of EVs and shoreline erosion when using a synthetic event, possibly owing to the fact that the approach over-estimated E and Tp, in general. The present study, however, evidenced a general under-estimation of the EV as shown in Figure 8. This was linked (Figure 9) to the more frequent under-estimation of P with the STSS, which is determined by under-estimation of E and Tp. Such differences between both studies reflect the use of a different approach to represent the storm evolution. Despite this, the differences between real- and synthetic-based outputs were smaller in Sánchez-Arcilla et al (2009) than those found in this study. However, to apply that approach, the shape of the event must be known *a priori* to mimic the storm evolution, whereas the STSS approach only requires storm bulk information. In addition to this, the number of cases simulated here to obtain a robust statistic of errors is much larger, and covers a wider range of conditions than in Sánchez-Arcilla et al (2009).

The apparent trend highlighted for the ΔEV-ΔE and ΔEV-ΔTp relationships, agrees with the findings of McCall et al. (2010). In that work, the authors performed a sensitivity analysis of a 2D XBeach model of the barrier island of Santa Rosa (FL, US), varying the synthetic symmetric triangular Hs, and the Tp time-series of the Hurricane Ivan event (the base case) by the 30%. Notably, the variation introduced on the wave time-series of the base case did not influence its symmetric triangular shape. An analysis of the morphological impact on a foredune area showed that, in addition to expected changes in the EV following changes in Hs (and thus, E), the varying Tp conditions (Mean and Peak ΔTp = ±30%) resulted, in the under-estimation (ΔEV ~-30%) and over-estimation (ΔEV ~18%) of the EV, respectively. However, the same study also concluded that the erosion model output was more sensitive to (some) sediment transport parameters than to varying hydrodynamic conditions. This suggests that the differences induced using triangular storms (or SSs, in general) can potentially be compensated for by a calibration process. However, as the results obtained in this study show both under- and over-prediction, deeper investigations are required to verify this hypothesis under a wide range of storm conditions.

The obtained results demonstrate the existence of a strong relation between differences in erosion and inundation hazards (see Figure 10). The differences in the EV (ΔEV) and the phase lag of the water discharge (ΔQD) are linked, confirming the importance of morphodynamic feedback when simulating coastal inundation. A good/reasonable agreement (between real and triangular storms) on the computed EV (|ΔEV|<20%) leads to a good agreement on the positioning of the peak of the water discharge (|ΔQD|<5%). This should be important when the interest is in accurately timing the peak of the floodwater volume. However, this fine reproduction of the peak timing does not necessarily imply that the total floodwater during the event will be accurately reproduced. In fact, the obtained results showed that a good reproduction of the EV (|ΔEV|<5%) is not accompanied by a good simulation of the inundation (|ΔTWV|<5%). Despite this, under- or over-estimation of erosion (|ΔEV|>5%) leads to strong under- or over-estimation of inundation (|TWV|>20%), respectively.

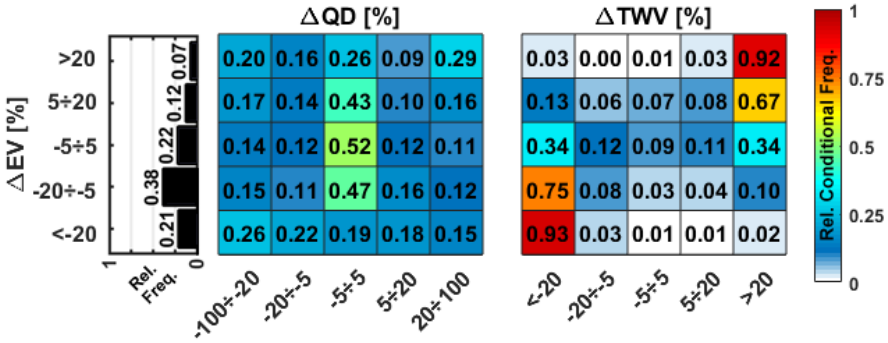

Figure 10. Relation between the ΔEV with the relative differences in flooding-related variables. The relative conditional frequency distributions are shown through coloured tables, where each row represents a conditioning range of ΔEV. From left to right: distribution of ΔEV for the whole dataset; conditional distributions of relative peak discharge delay (ΔQD); and total water volume relative difference (ΔTWV).

To determine if the previously-observed differences are related to the structure of simulated conditions, they were further analysed according to the energy of the storm, the profile conditions (dissipative or reflective), location (storm dataset), and WL (Figure 11). Focusing on the -20% to +20% range of uncertainty in the hazard estimation, the results presented in Section 3 are not strongly conditioned by any of the analysed conditions. Although a slightly better estimation of EVs is obtained for reflective conditions and extremely energetic storms, the obtained results are consistently homogeneous throughout the dataset, especially when looking at the relative differences between -5% and +5%.

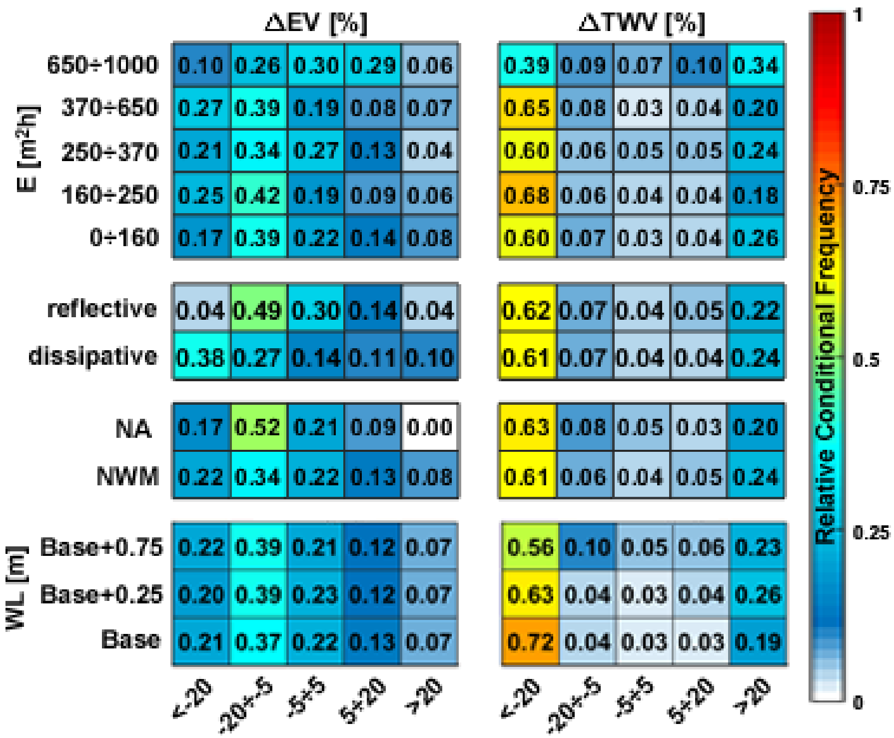

Figure 11. Relation between ΔEV (on the left) and ΔTWV (on the right) with (from top to bottom) the storm energy (E) class; the profile characteristics (reflective, dissipative); location (i.e. the storm sub-datasets: Northern Adriatic, NA; North-Western Mediterranean, NWM); and water level (WL). The relative conditional frequency distributions of ΔEV and ΔTWV are shown through coloured tables, where each row represents a different conditioning range of the analysed variables.

5 Conclusions

This study investigated the differences generated when simulating the hazard impacts of coastal storms using a STSS of waves, instead of the real data. It was demonstrated that the synthetic method, applied in an event-to-event manner, leads to highly uncertain and misleading deterministic hazard assessments, strongly limiting the reliability of the modelling approach.

After analysing the computed differences in reproducing storm-induced hazards by using STSSs, it can be concluded that they hardly reproduce the real magnitude with independence from the structure of storms or profiles. Differences in wave power are the dominant factor in transferring errors to hazards, and are determined by differences in storm energy (i.e., significant wave height) and period. These are mainly controlled by the adopted synthetic shape, which directly affects the synthetic significant wave height (and thus, energy), and indirectly affects wave period while calculating it with empirical predictive relations (i.e., Tp-Hs) applied to the synthetic wave heights; and secondarily, by the empirical predictive relations (i.e., Tp-Hs), which directly affects the synthetic period.

This is applicable to the range of simulated conditions, and permits one to conclude that although the use of STSSs adequately reproduces some of the main bulk variables defining the storm, they only reasonably reproduce the storm-induced hazard magnitude, i.e. accepting uncertainty in the order of (or greater than) +20% and -20%. Notwithstanding the fact that this type of synthetic approach has been used in recent projects and for engineering purposes, its use should be discouraged, whereas its results should be carefully discussed considering the shortcomings related to its use.

This highlights the need for further investigations towards a generalised synthetic approach that can optimise the simulation of coastal hazards, while minimizing the uncertainty related to the use of design events.

Conflict of interest statement. The authors declare that they have no known competing financial interests or personal relationships that could have appeared to influence the work reported in this paper.

CRediT authorship contribution statement. Enrico Duo: Conceptualization, Methodology, Software, Formal analysis, Investigation, Data Curation, , Writing - Review & Editing; Marc Sanuy: Conceptualization, Methodology, Software, Formal analysis, Investigation, Data Curation, , Writing - Review & Editing; José A. Jiménez: Conceptualization, Funding acquisition, Writing - Review & Editing, Supervision; Paolo Ciavola: Funding acquisition, Writing - Review & Editing, Supervision.

Acknowledgements. The authors thank: Eni and ARPA-ER for providing topo-bathymetric and wave data for the Italian site; the Institut Cartogràfic i Geológic de Catalunya for supplying topographic data, and IH-Cantabria for supplying wave and water level data for the Spanish site. The authors thank Clara Armaroli, Ap van Dongeren, Tom Spencer, Óscar Ferreira and Diego Vicinanza, for their valuable comments and suggestions at early stages of the manuscript preparation.

Funding. The work of E. Duo was supported by a PhD grant at the Department of Physics and Earth Science of the University of Ferrara, additional funding from the contribution “5 per mille assegnato all’Università di Ferrara - dichiarazione dei redditi dell’anno 2013” assigned through the "Bando Giovani Ricercatori 2016" of the University of Ferrara, and the EU H2020 ANYWHERE (GA 700099; www.anywhere-h2020.eu). The work of M. Sanuy and J.A. Jiménez has been done in the framework of the M-CostAdapt (CTM2017-83655-C2-1-R) research project (MINECO/AEI/FEDER, UE). Marc Sanuy was supported by a PhD grant from the Spanish Ministry of Education, Culture and Sport.

References

Armaroli, C. and Duo, E., 2018. Validation of the coastal storm risk assessment framework along the Emilia-Romagna coast. Coast. Eng. 134, 159–167. https://doi.org/10.1016/j.coastaleng.2017.08.014

Armaroli, C., Ciavola, P., Perini, L., Calabrese, L., Lorito, S., Valentini, A., and Masina, M., 2012. Critical storm thresholds for significant morphological changes and damage along the Emilia-Romagna coastline, Italy, Geomorphology, 143–144, 34–51. https://doi.org/10.1016/j.geomorph.2011.09.006

Boccotti, P., 2000. Wave Mechanics for Ocean Engineering. Elsevier Science, Oxford.

Bromirski, P.D., and Cayan, D.R. (2015). Wave power variability and trends across the N orth Atlantic influenced by decadal climate patterns. J. Geophys. Res. Oceans. 120(5), 3419-3443. https://doi.org/10.1002/2014JC010440

Burvingt, O., Masselink, G., Russell, P., Scott, T., 2017. Classification of beach response to extreme storms. Geomorphology, 295, 722-737. https://doi.org/10.1016/j.geomorph.2017.07.022

Callaghan, D.P., Ranasinghe, R., Short, A., 2009. Quantifying the storm erosion hazard for coastal planning. Coast. Eng. 56, 90–93. https://doi.org/10.1016/j.coastaleng.2008.10.003

Camus, P., Mendez, F.J., Medina, R., Tomas, A., and Izaguirre, C., 2013. High resolution downscaled ocean waves (DOW) reanalysis in coastal areas. Coast. Eng. 72, 56–68. https://doi.org/10.1016/j.coastaleng.2012.09.002

Carley, J.T., Cox, R.J., 2003. A methodology for utilising time-dependent beach erosion models for design events, in: Kench, P.S., Hume, T.M. (Eds.), Coasts & Ports 2003 Australasian Conference: Proceedings of the 16th Australasian Coastal and Ocean Engineering Conference, the 9th Australasian Port and Harbour Conference and the Annual New Zealand Coastal Society Conference, Auckland, New Zealand, 9-1. Institution of Engineers, Australia, pp. 587–595.

Corbella, S. and Stretch, D.D., 2012a. Multivariate return periods of sea storms for coastal erosion risk assessment. Nat. Hazards Earth Syst. Sci. 12, 2699–2708. https://doi.org/10.5194/nhess-12-2699-2012

Corbella, S., and Stretch, D.D., 2012b. Predicting coastal erosion trends using non-stationary statistics and process-based models. Coast. Eng. 70, 40–49. https://doi.org/10.1016/j.coastaleng.2012.06.004

Corbella, S., and Stretch, D.D., 2013. Simulating a multivariate sea storm using Archimedean copulas. Coast. Eng. .76, 68-78. https://doi.org/10.1016/j.coastaleng.2013.01.011

Duo, E., Trembanis, A. C., Dohner, S., Grottoli, E., and Ciavola, P., 2018. Local-scale post-event assessments with GPS and UAV-based quick-response surveys: a pilot case from the Emilia–Romagna (Italy) coast. Nat. Hazards Earth Syst. Sci. 18, 2969-2989. https://doi.org/10.5194/nhess-18-2969-2018

Fedele, F., and Arena, F., 2009. The equivalent power storm model for long-term predictions of extreme wave events. Proc. of the 28th International Conference on Ocean, Offshore and Arctic Engineering (OMAE 2009). American Society of Mechanical Engineers (ASME). https://doi.org/10.1115/OMAE2009-79597

Gallien, T.W., Kalligeris, N., Delisle, M.-P.C., Tang, B.-X., Lucey, J.T.D., Winters, M.A., 2018. Coastal flood modeling challenges in defended urban backshores. Geosciences, 8, 450. https://doi.org/10.3390/geosciences8120450

Harley, M.D., Valentini, A., Armaroli, C., Perini, L., Calabrese, L., Ciavola, P., 2016. Can an early-warning system help minimize the impacts of coastal storms? A case study of the 2012 Halloween storm, northern Italy. Nat. Hazards Earth Syst. Sci. 16, 209–222. https://doi.org/10.5194/nhess-16-209-2016

Jäger, W.S., Nagler, T., Czado, C., and McCall, R.T., 2019. A statistical simulation method for joint time series of non-stationary hourly wave parameters. Coast. Eng. 146, 14–31. https://doi.org/10.1016/j.coastaleng.2018.11.003

Jiménez, J. A., Sanuy, M., Ballesteros, C. and Valdemoro, H. I., 2018. The Tordera Delta, a hotspot to storm impacts in the coast northwards of Barcelona (NW Mediterranean). Coast. Eng. 134, 148-158. https://doi.org/10.1016/j.coastaleng.2017.08.012

Laface, V., and Arena, F., 2016. A new equivalent exponential storm model for long-term statistics of ocean waves. Coast. Eng. 116, 133-151. https://doi.org/10.1016/j.coastaleng.2016.06.011

Laface, V., Malara, G., Romolo, A., Arena, F., 2016. Peak over threshold vis-à-vis equivalent triangular storm: Return value sensitivity to storm threshold. Coast. Eng. 116, 220-235. https://doi.org/10.1016/j.coastaleng.2016.06.009

Larson, M., and Kraus, N.C., 1989. SBEACH: Numerical Model for Simulating Storm-Induced Beach Change - Report 1: Empirical Foundation and Model Development. Technical Report CERC- 89-9, Coastal Engineering Research Center, Water- ways Experiment Station, Vicksburg, Mississippi. https://doi.org/10.5962/bhl.title.47893

Lin-Ye, J., Garcia-Leon, M., Garcia, V., and Sánchez-Arcilla, A., 2016. A multivariate statistical model of extreme events: An application to the Catalan coast. Coast. Eng. 117, 138–156. https://doi.org/10.1016/j.coastaleng.2016.08.002

Lira-Loarca, A., Cobos, M., Losada, M.A., and Baquerizo, A., 2020. Storm characterization and simulation for damage evolution models of maritime structures. Coast. Eng. 156, 103620. https://doi.org/10.1016/j.coastaleng.2019.103620

Martín-Hidalgo, M., Martín-Soldevilla, M.J., Negro, V., Aberturas, P., and López-Gutiérrez, J.S., 2014. Storm evolution characterization for analysing stone armour damage progression. Coast. Eng. 85, 1–11. https://doi.org/10.1016/j.coastaleng.2013.11.008

Martín-Soldevilla, M.J., Martín-Hidalgo, M., Negro, V., López-Gutiérrez, J.S., and Aberturas, P., 2015. Improvement of theoretical storm characterization for different climate conditions. Coast. Eng. 96, 71–80. https://doi.org/10.1016/j.coastaleng.2014.11.004

Masina, M., and Ciavola, P., 2011. Analisi dei livelli marini estremi e delle acque alte lungo il litorale ravennate. Studi Costieri 18, 87–101.

Mathiesen, M., Goda, Y., Hawkes, P. J., Mansard, E., Martín, M. J., Peltier, E., Thompson, E. F. and Van Vledder, G., 1994. Recommended practice for extreme wave analysis. J. Hydraul. Res. 32(6), 803–814. https://doi.org/10.1080/00221689409498691

McCall, R.T., Van Thiel de Vries, J.S.M., Plant, N.G., Van Dongeren, A.R., Roelvink, J.A., Thompson, D.M., Reniers, A.J.H.M., 2010. Two-dimensional time dependent hurricane overwash and erosion modeling at Santa Rosa Island. Coast. Eng. 57, 668–683. https://doi.org/10.1016/j.coastaleng.2010.02.006

Mendoza, E. T., Jimenez, J. A. and Mateo, J., 2011. A coastal storms intensity scale for the Catalan sea (NW Mediterranean). Nat. Hazards Earth Syst. Sci. 11, 2453–2462. https://doi.org/10.5194/nhess-11-2453-2011

Nielsen, A.F., Adamantidis, C.A., 2007. Defining the Storm Erosion Hazard for Beaches. Aust. J. Civ. Eng. 3, 39–50. https://doi.org/10.1080/14488353.2007.11463920

Passeri, D.L., Bilskie, M.V., Plant, N.G., Long, J.W. and Hagen, S.C., 2018. Dynamic modeling of barrier island response to hurricane storm surge under future sea level rise. Climatic Change 149(3-4), 413-425. https://doi.org/10.1007/s10584-018-2245-8

Plomaritis, T.A., Costas, S., Ferreira, Ó., 2017. Use of a Bayesian Network for coastal hazards, impact and disaster risk reduction assessment at a coastal barrier (Ria Formosa, Portugal). Coast. Eng. 134, 134-147. https://doi.org/10.1016/j.coastaleng.2017.07.003

Poelhekke, L., Jäger, W.S., van Dongeren, A., Plomaritis, T.A., McCall, R., Ferreira, Ó., 2016. Predicting coastal hazards for sandy coasts with a Bayesian Network. Coast. Eng. 118, 21–34. https://doi.org/10.1016/j.coastaleng.2016.08.011

Ranasinghe, R., Callaghan, D., 2017. Assessing Storm Erosion Hazards, in: Ciavola, P., Coco, G. (Eds.), Coastal Storms: Processes and Impacts. John Wiley & Sons Ltd., pp. 241–256.

Reguero, B.G., Menéndez, M., Méndez, F.J., Mínguez, R. and Losada, I.J., 2012. A Global Ocean Wave (GOW) calibrated reanalysis from 1948 onwards. Coast. Eng. 65, 38-55. https://doi.org/10.1016/j.coastaleng.2012.03.003

Roelvink, D., Reniers, A., 2012. A guide to modeling coastal morphology. World Scientific Publishing Co. Pte. Ltd. https://doi.org/10.1142/9789814304269

Roelvink, D., Reniers, A., van Dongeren, A., van Thiel de Vries, J., McCall, R., Lescinski, J., 2009. Modelling storm impacts on beaches, dunes and barrier islands. Coast. Eng. 56, 1133–1152. https://doi.org/10.1016/j.coastaleng.2009.08.006

Sánchez-Arcilla, A., Mendoza, E.T., Jiménez, J.A., Peña, C., Galofré, J., Novoa, M., 2009. Beach Erosion and Storm Parameters: Uncertainties for the Spanish Mediterranean., in: McKee Smith, J. (Ed.), Coastal Engineering 2008 Proceedings of the 31st International Conference Hamburg, Germany, 31 August – 5 September 2008. World Scientific, pp. 2352–2362. https://doi.org/10.1142/9789814277426_0194

Santos, V.M., Wahl, T., Long, J.W., Passeri, D.L., and Plant, N. G., (2019). Combining numerical and statistical models to predict storm-induced dune erosion. J. Geophys. Res. Earth Surf. 124, 1817–1834. https://doi.org/10.1029/2019JF005016

Sanuy, M., Duo, E., Jäger, W.S., Ciavola, P., Jiménez, J.A., 2018. Linking source with consequences of coastal storm impacts for climate change and risk reduction scenarios for Mediterranean sandy beaches. Nat. Hazards Earth Syst. Sci. 18, 1825–1847. https://doi.org/10.5194/nhess-18-1825-2018

Sanuy M., Jiménez J.A., Ortego M.I., Toimil A., 2019. Differences in assigning probabilities to coastal inundation hazard estimators: Event versus response approaches. J. Flood Risk Management. e12557. https://doi.org/10.1111/jfr3.12557

Solari, S., and Losada, M.A., 2018. Simulation of sea storms including multivariate storm evolution. Proc. 36th Int. Conf. on Coast. Eng. ASCE, papers.35. https://doi.org/10.9753/icce.v36.papers.35

Vousdoukas, M.I., Ferreira, Ó., Almeida, L.P. and Pacheco, A., 2012. Toward reliable storm-hazard forecasts: XBeach calibration and its potential application in an operational early-warning system. Ocean Dynamics 62(7), 1001-1015. https://doi.org/10.1007/s10236-012-0544-6

Williams, J.J., Esteves, L.S. and Rochford, L.A., 2015. Modelling storm responses on a high-energy coastline with XBeach. Model. Earth Syst. Environ. 1:3. https://doi.org/10.1007/s40808-015-0003-8